Volume 1 | Number 1 | Jan 2013 | Pages 1–100

Nanoscale

www.rsc.org/nanoscale

ROYAL SOCIETY OF CHEMISTRY

ROYAL SOCIETY OF CHEMISTRY

www.rsc.org/nanoscale

Nanoscale

ARTICLE

Site-Specific Growth of Pt shell on Au nanoplates: tailoring their surface plasmonic behavior

Hee-Jeong Jang,[a] Soonchang Hong,[a] Songyi Ham,[a] Kevin L. Shuford,*[,c] and Sungho Park*[,a,b]

In this report, we tune the surface plasmonic behavior of Au nanoplates depending on the morphology of Pt shell in which Pt is considered as less optically inactive element. We describe the synthesis of flat Au nanoplates coated with Pt via rim-preferential or uniform growth methods. Depending on the site-selective growth of Pt on core Au nanoplates, the aspect ratio of the resulting Au@Pt nanoplates was tunable and their corresponding surface plasmon resonance (SPR) bands were controlled accordingly. Although Pt is regarded as an optically weak component in visible and near infrared spectral windows, a Pt coating affects the SPR behavior of core Au nanoplates due to effective surface plasmon (SP) coupling between the core Au and deposited Pt shell. We systematically investigated the optical properties of uniformly grown (Au@Pt(uni)) and rim-preferentially grown (Au@Pt(rim)) Au@Pt nanoplates by observing their SPR band shifts compared to SPR of Au nanoplates. Due to the structural rigidity conferred by the Pt coating, the Au@Pt nanoplates can be easily transferred to the investigated solvents

1 Introduction

Shape control of nanocrystals has gained continuous attention due to their interesting shape-dependent catalytic[1-8] and optical[9-15] properties. Site-selective growth[16-21] is an important issue in preparing appropriate nanostructures for a variety of targeted purposes. Au nanostructures are a representative candidate for optical sensor applications due to their strong surface plasmon resonance (SPR) in visible and near infrared spectral windows[21-24] and excellent optical tunability that is achievable by controlling the shape and size. A variety of synthetic methods for Au nanostructures[25-28] allow tuning of the absorption band in the range from visible to near infrared wavelengths by changing the shape and size of nanocrystals. Au nanoplates[23] are well known to have strong SPR properties. However, they have weak structural stability in that the Au aggregates are easily formed due to their ductility. In contrast to spherical NPs, NPs with a plate-like shape are thermodynamically unstable because the exposed surface area is much larger than that of spherical NPs. The large flat facets can readily form large areas of interfacial contact among nanoplates, and therefore nanoplates are likely to transform into aggregated conglomerates to reduce the exposed outer surface area.

We chose Pt as a shell component in order to complement the structural instability of the Au core. In the Au@Pt plate-like nanostructure, Au nanoplates show strong SPR properties and the plate-like morphology provides much stronger interaction with surrounding medium than their spherical counterpart due to their larger exposed surface area with respect to the total mass. Although the Pt component has weak optical properties, the strong SPR properties of Au could complement the optically less active Pt shell via surface plasmon (SP) coupling.[30, 31] In the case of metal nanostructures, SPR occurs on the whole parts of nanostructure and at the interface or junction between two metals under electromagnetic radiation via SP coupling. Recently, SP coupling has been intensely investigated for multi-component or multi-block nanostructures consisting of optically active Au or Ag,[27] and even for nanorods composed of Ni,[32] which is much less optically active than Au or Ag. For Au and Pt systems, we investigated the SP coupling within multiblock Au-Pt nanorods.[31] The larger portion of Au helps the SP coupling between Au and Pt blocks, leading to the similar appearance of SPR modes observable from pure Au nanorods. This previous work motivated us to scrutinize the SP coupling on other more complex nanostructures consisting of Au and Pt.

For the observation of SP coupling between Au and Pt, colloidal nanorods structures, especially core-shell Au@Pt nanorods, have been frequently chosen by other researchers. Liz-Marzan group studied synthesis methods[33] and optical properties[34] of Pt-coated Au nanorods. They systematically characterized the optical shifting tendency depending on homogeneous coating and tip coating of platinum on Au nanorods. Homogeneous

coating of Pt on Au nanorods induced slight blueshifting of the longitudinal band in the optical spectra, while tip coating of Pt made the Au@Pt nanorods undergo a redshift.[30, 33, 34] In the research studied by Xie group,[30] Au@Pt nanorods have higher dielectric sensitivity than pure Au nanorods with the same dimension.

In this study, we applied two methodologies for the site-selective growth of Pt on Au nanoplates, dubbed rim-preferential growth and uniform growth. The plate-like Au@Pt core-shell nanostructures have not been thoroughly examined yet when it comes to SP coupling between Au and Pt. We systematically investigated the optical properties of uniformly grown (Au@Pt(uni)) and rim-preferentially grown (Au@Pt(rim)) Au@Pt nanoplates by observing their SPR band shifts. In addition, the stability of Au@Pt nanoplates was confirmed in ambient condition and in several solvents.

2 Results and discussion

Characterization of Rim-preferential Growth and Uniform Growth of Pt
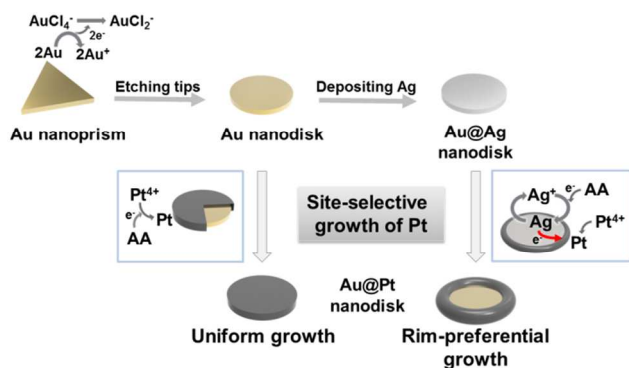
Scheme 1. Schematic illustration of the experimental precedures regarding rim-preferential growth and uniform growth of Pt on Au nanoplates

We synthesized flat Au@Pt core-shell nanoplates with different morphologies via rim-preferential and uniform growth techniques (Scheme 1). Uniform growth means that Pt is coated uniformly on the core Au nanoplates, while rim-preferential growth refers to the complex shape where Pt is selectively reduced only at the rim part of the Au nanoplate. In this experiment, Au nanodisks used as a seed for depositing Pt are prepared by etching tips of Au nanoprisms. As mentioned in the literature[42], we added aqueous solution containing Au^{3+} ions in nanoprism solution, and observed UV-vis spectra to confirm the transformation from nanoprism to nanodisk. The existence of thin Ag layer on Au nanoplates determines the growth mode of Pt shell. The mechanism of rim-preferential growth was suggested in our previous report.[35] The thin Ag layer on the Au nanoplates plays an important role in the deposition of platinum atoms selectively at the rim, which is facilitated by electron shuttling through Ag layer. Once Pt atoms are reduced at the rim, the site having high surface energy, the more electrons from the Ag layer flow to initial nucleation site of Pt through the remained Ag layer and Au plate. This process ends up after exhaustion of Pt precursor, since excess amount of ascorbic acid allows the Ag layer to recycle. In the absence of a thin Ag layer, the uniform growth of Pt occurred over the entire Au nanoplates. We synthesized two different Au@Pt nanoplate

structures in a straightforward manner, Au@Pt(uni) and Au@Pt(rim) nanoplates, in the absence and presence of a thin Ag layer, respectively.
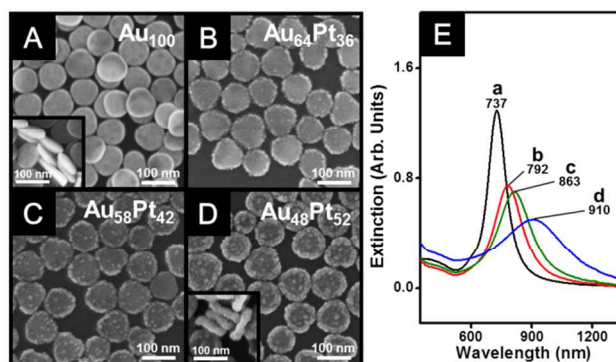
Fig. 1. FESEM images of Au nanodisks (A), rim-preferentially Pt-coated Au nanodisks (Au@Pt(rim) nanodisks) (B-D) as increasing the concentration of Pt precursors. Atomic percent of Au and Pt is indicated at the upper right side of each image, which is obtained from EDS analysis. The insets are their side view (A and D, inset) (E) UV-vis-NIR spectra of Au nanodisks (line a), Au@Pt(rim) nanodisks (line b, c, and d). The line a, b, c, and d correspond to the SEM images in (A-D), respectively. The wavelength of SPR peaks is shown on the top of each peak.

We characterized the structure and optical properties of Au@Pt(rim) and Au@Pt(uni) nanodisks using FESEM, UV-vis-NIR spectroscopy, and TEM. In a typical experiment, the preferential deposition of Pt at the rim of the Au nanodisks was systematically monitored by FESEM images, as shown in Fig. 1. The Au@Pt(rim) nanodisks (Fig. 1B-D) were synthesized using Au nanodisks (Fig. 1A) as a seed. Pt-coated Au nanocrystals usually have a bumpy surface due to lattice mismatch.[36] As the concentration of Pt precursors in the growth solution increased, the thickness of the Pt layer formed at the rim of the Au nanodisks increased. The diameter of each nanodisk was 88 ± 5 nm (Fig. 1A), 94 ± 8 nm (Fig. 1B), 97 ± 7 nm (Fig. 1C), and 101 ± 8 nm (Fig. 1D), while their rim thicknesses were 11 ± 1 nm, 21 ± 3 nm, 29 ± 2 nm, and 35 ± 3 nm, respectively. The atomic percent of Au to Pt was obtained from energy dispersive X-ray spectrometry (EDS) analysis and is shown on the upper right side of each SEM image. The concentration of Pt precursors in the growth solution is proportional to the total number of deposited Pt atoms. Thicker Pt rims could be obtained as the amount of Pt precursor present in the growth solution increased.

The corresponding SPR bands are displayed in Fig. 1E. The pure Au nanodisks showed their representative in-plane dipole mode at 737 nm. As the thickness of the Pt rims increased, the SPR bands shifted toward a longer wavelength. The Au@Pt(rim) nanodisks (corresponding to the images shown in Fig. 1B-D) showed their peak maximum at 792, 863, and 910 nm, respectively. The observed SPR shifting trend is similar to previous results obtained from dumbbell-shaped or arrow-headed Au nanorods[37, 38] and tip-coated Au@Pt nanorods[33, 34]. In the case of nanorods, the longitudinal mode of SPR bands is dictated by the aspect ratio (AR_{rod} = length / diameter). When reduction of Au or Pt ions occurs on the tips of the Au nanorods, the increase in the AR_{rod} leads to a redshift of the SPR bands. In the case of nanoplates, the increase in the aspect ratio (AR_{prism} = edge length / thickness, AR_{disk} = diameter / thickness) also leads to a redshift of the SPR bands.[41] In the case of dogbone-like Au nanorods, the position of the

longitudinal plasmon is more strongly influenced by the aspect ratio_mid ($AR_{rod-mid}$ = length / diameter of the mid-section) rather than the aspect ratio_max ($AR_{rod-max}$ = length / maximum diameter of the ends).[37] Careful attention is needed in the comparison of aspect ratios between rods and plates in that the diameter of nanorods is the shorter axis, while the diameter of nanodisks is the longer axis. In the case of our Au@Pt(rim) nanodisk, the preferential deposition of Pt at the rim led to an increase in the total diameter of the nanodisk. The central part retained its original thickness and therefore the preferential deposition of Pt at the rim eventually led to an increase in the $AR_{disk-mid}$ (diameter / thickness of the mid-section). Given that SP coupling occurs between the core Au nanodisk and the Pt rim, it is expected that the increase in aspect ratio would result in a peak shift to a longer wavelength. Pt is usually regarded as a less optically active component in the visible-NIR spectral window. Unless there is SP coupling between Au and Pt, the resulting SPR bands will not show any peak-shifting, but stay at the same wavelength as that of pure Au nanoplates only with slight damping. However, the observed SPR bands showed redshifting as well as a well-defined bands in spite of Pt component, which resulted from their effective SP coupling.
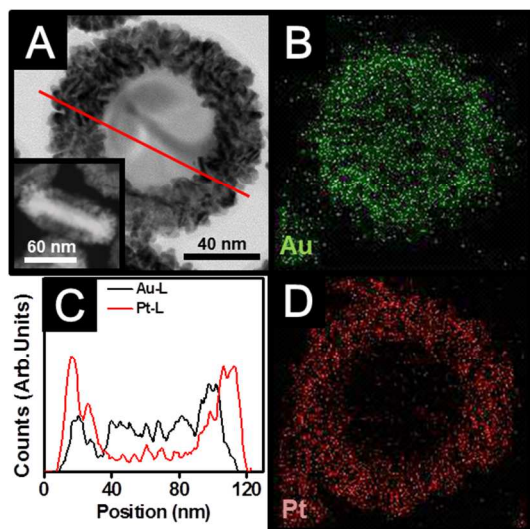
Fig. 2. (A) A TEM image of Au@Pt(rim) nanodisks (the inset, showing the side view of Au@Pt(rim) nanodisks). (B, D) EDS elemental mapping images of (B) Au element distribution and (D) Pt element distribution corresponding to the image (A). (C) EDS line mapping of Au@Pt(rim) nanodisks in which the red line represents the amount of Pt atoms, and the black line is the amount of Au atoms. The mapping was conducted along the red line in (A).
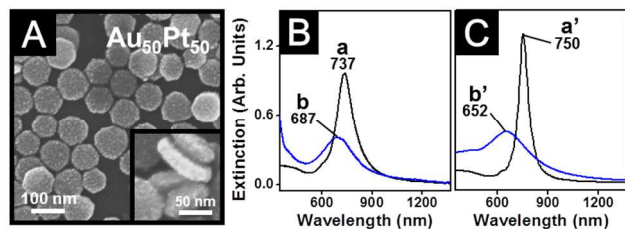
Fig. 3. (A) A FESEM image of Au@Pt(uni) nanodisks. Atomic percent obtained from EDS analysis is shown at the upper right side of the image. The inset FESEM image is the side view of Au@Pt(uni) nanodisks. (B) UV-vis-NIR spectra of Au nanodisks (line a) and Au@Pt(uni) nanodisks (line b). The wavelength of SPR peaks is indicated on the top of each peak. (C) Calculated spectra corresponding to Au@Pt(uni) nanodisks with the same dimension used in experimental data.
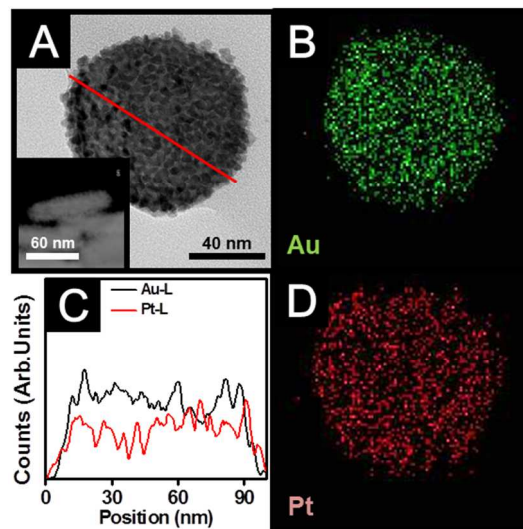
Fig. 4. (A) A TEM image of Au@Pt(uni) nanodisks. The insets show the side view of Au@Pt(uni) nanodisks. (B, D) EDS elemental mapping images of Au@Pt(uni) nanodisks of (B) Au element distribution and (D) Pt element distribution. (C) EDS line mapping of Au@Pt(uni) nanodisks (black line : Au element, red line : Pt element). The mapping was conducted along the red line in (A).

A detailed structural analysis of the Au@Pt(rim) nanodisks was carried out by TEM as exhibited in Fig. 2. The darker region indicates the thicker deposition of Pt at the rim (Fig. 2A), and the side view provides the thickness profile (Fig. 2A, inset). TEM elemental mapping (Fig. 2B and D) showed that the Au atoms were homogeneously distributed around the central region, while the Pt atoms were mainly located at the rim of the nanodisks. Fig. 2C shows the TEM line mapping along the red line in Fig. 2A. The resultant profile shows a higher concentration of Pt at the rim than in the central region. As a comparison, Au@Pt(uni) nanodisks were investigated using SEM, UV-vis-NIR spectroscopy, and TEM. Panel A of Fig. 3 shows the uniform coating of Pt on the core Au nanodisk. The resulting Au@Pt(uni) nanodisks had a bumpy Pt granular deposition over the entire Au nanodisk due to lattice mismatch between the Pt and Au. When there was no Ag coating on the Au nanodisk, Pt ion reduction occurred on the Au surface without facet preference. In the typical experiment, the diameter of the Au nanoplate changed from 88 ± 5 nm (before Pt deposition) to 92 ± 7 nm (after Pt deposition), and the thickness increased from 11 ± 1 nm to 22 ± 3 nm.

In contrast to the case of Au@Pt(rim) nanodisks, the corresponding SPR band shifted to a shorter wavelength from 737 nm to 687 nm (Fig. 3B). The resulting blueshift originates from the decrease in aspect ratio from 8.0 to 4.2. In Fig. 3C, we carried out theoretical calculation by using discrete dipole approximation (DDA).[39, 40] The DDA calculation shows similar tendency of peak shifting with the experimental results (Fig. 3C).

The TEM image (Fig. 4A) revealed that Pt was uniformly coated on the Au nanoplates, and the side view (Fig. 4A, inset) indicated that the Au@Pt(uni) nanoplates had a relatively flat, but still bumpy surface, without any preferential deposition. Both TEM elemental mapping (Fig. 4B and D) and EDS line mapping (Fig. 4C) confirmed the homogeneous coating of Pt over the entire Au nanodisk without facet selectivity. The EDS line mapping analysis was conducted along the red line shown in Fig. 4A.

Confirmation of Reaction Tendency on Triangular Nanoplates
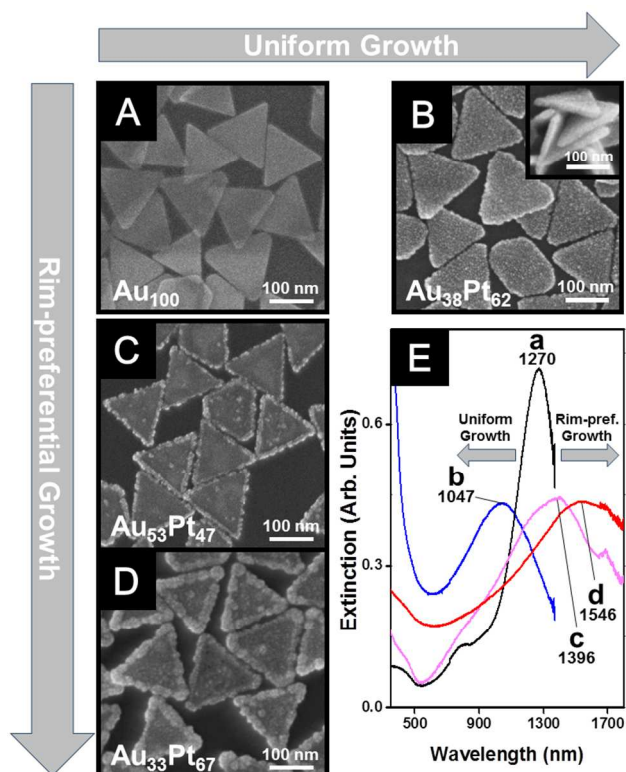
Fig. 5. (A-D) FESEM images of (A) Au nanoprisms, (B) Au@Pt(uni) nanoprisms, (C-D) Au@Pt(rim) nanoprisms. Atomic percent from EDS analysis is shown at the lower left side of each image. (E) UV-vis-NIR spectra of Au nanoprisms (line a), Au@Pt(uni) nanoprisms (line b), and Au@Pt(rim) nanoprisms (line c and d) corresponding to the FESEM images (A-D).

In order to test the generality of the aforementioned synthetic strategy toward different shapes of Au nanoplates other than nanodisks, we synthesized triangular Au@Pt nanoprisms. As demonstrated in Fig. 5A-D, uniform or rim-preferential coating of Pt was possible on the Au nanoprisms. Therefore, the suggested synthetic strategy was applicable to flat Au nanoplates without shape discrimination. The FESEM images showed that the edge length of the Au nanoprisms was initially 155 ± 8 nm (panel A) and decreased slightly to 147 ± 11 nm (panel B) when Pt was homogeneously coated over the entire Au nanoprisms. The edge length increased to 162 ± 7 nm and 181 ± 13 nm as Pt reduction occurred selectively on the edge of the Au nanoprisms (panels C and D). The measured thickness also increased from 9 ± 1 nm (Au nanoprism) to 11 ± 1 nm (Au@Pt(uni) nanoprisms, in panel B), 13 ± 1 nm (Au@Pt(rim) nanoprisms, in panel C), and 27 ± 3 nm (Au@Pt(rim) nanoprisms, in panel D). As in the case of the Au@Pt nanodisks, the optical behavior of the Au@Pt nanoprisms showed a dependence on the variation in aspect ratios. AR_{prism} decreased from 17 (Au nanoprism)to 13 (Au@Pt(uni) nanoprism), and accordingly the in-plane dipole mode of the Au nanoprisms at 1270 nm blueshifted to 1047 nm. In contrast, the AR_{prism} increased from 17 (Au nanoprism) to 18 and 20 ($AR_{prism-mid}$ = edge length / thickness of the mid-section), and the SPR peak position redshifted from 1270 nm to 1396 nm and 1546 nm, respectively. The SPR bands of the Au@Pt plate-like nanostructure are tunable in the range from 700 to 1800 nm.

Stability and Dielectric Sensitivity of Au@Pt Nanoplates
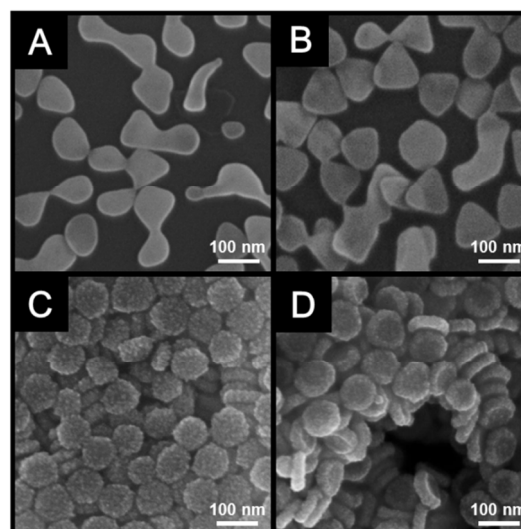
Fig. 6. FESEM images of (A) Au nanodisks and (B) Au nanoprisms left at ambient condition for 2 hours after sampling, and (C) Au@Pt(uni) nanodisks and (D) Au@Pt(rim) nanodisks left at ambient condition for 2 months after sampling.

Additionally, the unique advantage of the Au@Pt plate-like nanostructure compared to bare Au nanoplates is its high structural stability under drastic changes in the surrounding medium. In order to test their stability, we compared the FESEM images of bare Au nanodisks, Au nanoprisms, and Au@Pt nanoplates that were left under ambient conditions after solvent drying (Fig. 6). Bare Au nanodisks and nanoprisms aggregated with each other and their original shape was destroyed within two hours (Fig. 6A and B). However, the Au@Pt nanoplates retained their original shape without aggregation even after two months (Fig. 6C and D). In this observation, the difference between disks and prisms toward aggregation is negligible, so the aggregation of Au nanoplates easily occurs under non-aqueous condition regardless of the shape. Therefore, the increased stability of Au@Pt nanoplates is caused by Pt coating.
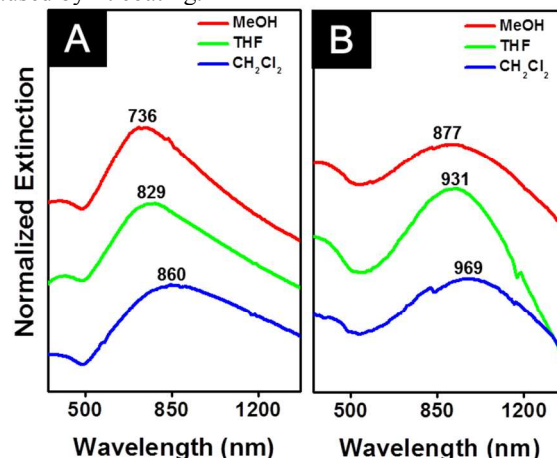
Fig. 7. UV-vis-NIR spectra of (A) Au@Pt(uni) nanodisks, and (B) Au@Pt(rim) nanodisks. Each spectrum was measured with changing the solvent having different refractive index, such as methanol, tetrahydrofuran, and CH_2Cl_2.

In order to confirm re-dispersion of Au@Pt nanoplates in several solvents, we obtained optical spectra. The solvents we

chose are methanol, tetrahydrofuran (THF), and CH_2Cl_2. The SPR bands of Au@Pt nanoplate in each solvent are shown in Fig. 7. Before re-dispersion in each solvent, all the samples are fully dried. The refractive index of methanol, THF, and CH_2Cl_2 is 1.329, 1.407, and 1.424, respectively. For all investigated samples, the SPR band redshifted as the refractive index of the solvent increased, which is consistent with other results reported in the literature.[10,16,30] In order to confirm the reliability of UV-vis spectra, we conducted several measurements on the same sample in organic solvent (Electronic supplementary Information, Fig. S1). Within three-time measurements, the wavelength of peak is changed by only 2 nm. Even after sonication, the peak position is just shifted by 4 nm. Since the aggregation occurs randomly, if nanoplates aggregated, the peak position would be fluctuated. The consistence of peak position means that serious aggregation does not occur. SEM images taken after transferring to toluene also show exact same structure maintaining the original shape (Fig. S2). Therefore, it was possible to directly transfer and re-disperse the Au@Pt nanoplates in any solvent.

3 Conclusions

We were able to tune the SPR bands of Au@Pt nanoplates by controlling the selective deposition of Pt on Au nanoplates via uniform or rim-preferential growth. The suggested synthetic strategy was applicable to Au nanodisks and nanoprisms. The SPR band shifts were dictated by aspect ratio variation depending on uniform or rim-preferential Pt growth onto core Au nanoplates. This result indicates that there is effective SP coupling between Au and Pt, although Pt is regarded as an optically weak metal in the visible-NIR spectral window. Due to the strong SPR properties of Au and the structural rigidity conferred by the addition of Pt, Au@Pt nanoplates can be easily transferred to the investigated solvents. We expect the site-selective control of Pt coating can be applied to the fine-tuning of surface plasmon bands, and eventually to the field of energy harvesting and biomedical application.

4 Experimental details

4. 1 Materials

All chemicals were used without further purification. Hydrogen tetrachloroaurate (III) hydrate ($HAuCl_4 \cdot nH_2O$, 99 %) was purchased from Kojima. Tri-sodium citrate dihydrate ($Na_3C_6H_5O_7 \cdot 2H_2O$, 99 %) was purchased from Yakuri. Sodium tetrahydroborate ($NaBH_4$, 98 %) and silver nitrate ($AgNO_3$, 99.8 %) were purchased from Junsei. Sodium iodide (NaI, 99.5 %) and L-ascorbic acid ($C_6H_8O_6$, 99.5 %) were purchased from Sigma Aldrich. Sodium hydroxide (NaOH, 98 %) was purchased from Samchun, and cetyl trimethyl ammonium bromide (CTAB, $C_{19}H_{42}BrN$, 95 %) was supplied by Fluka. All reagents were dissolved in distilled water (18.2 MΩ) that was prepared with a Milli-Q water purification system.

4. 2 Synthetic procedures

Au nanoprisms[41] were prepared from 5 nm spherical seeds by a three-step, seed-mediated method with iodide ions, as reported previously. Au nanodisks[42] were synthesized by conducting

further procedures with Au triangular nanoplates (experimental details are written in ESI). All of the gold nanoplate solutions were optically normalized to the same concentration. In the presence of iodide ions (50 μM), 20 mL of 50 mM CTAB, 5 mL of re-dispersed gold nanoplates, 340 μL of 0.1 M NaOH, and 54 μL of 2 mM aqueous $AgNO_3$ solution were added to a vial. To ensure uniform growth of Pt, we omitted the addition of $AgNO_3$ solution. Next, 426 μL of 10 mM ascorbic acid was added to the mixture. After gentle shaking, the solution was heated to 70 °C and kept in an oven to facilitate the deposition of Ag layers onto the Au nanoplates. After one hour, 135 μL, 270 μL, and 540 μL of 2 mM aqueous H_2PtCl_6 solution was added to the heated mixture for the galvanic replacement reaction, and the mixture was kept at 70 °C for approximately 3 hours. After the end of the reaction, we used a centrifuge and removed the supernatant to redisperse in DI water. This washing process repeated twice.

For transferring Au@Pt nanoplates to the other solvent, we fully dried the solution of nanoplates using a rotary evaporator, and dispersed nanoplates in the other solvent by ultrasonication.

4. 3 Characterization

A JEM-2100F was used to acquire transmission electron microscopy (TEM) images. Scanning electron microscopy (SEM) images were obtained using a JEOL 7000F and a JEOL 7600F. UV-vis-NIR absorption spectra were acquired using S-3100 (Scinco) and UV-3600 (Shimadzu) spectrophotometers.

4. 4 DDA calculation

We have performed discrete dipole approximation (DDA) calculations for Au@Pt(uni) nanodisks to confirm the interpretation of the experimental spectra. All calculated extinction spectra are for the nanoparticle embedded in a uniform dielectric medium corresponding to water. The spectra presented in the manuscript have been averaged over orientations to represent the optical properties of the particle in solution. The nanoparticle morphologies used in the calculations were based upon the SEM images and experimentally determined dimensions. In particular, for the solid Au nanodisk, the diameter was 88 nm and the thickness was 11 nm. For the Au@Pt(uni) nanodisk, the solid Au nanodisk was coated by a Pt layer, making the full particle diameter 92 nm and the thickness 22 nm. Custom input files were created that designate particle morphology and material by grid location. A 1 nm dipole spacing was used for all calculations. (experimental details are written in ESI)

Notes and references

[a]Department of Chemistry and [b]Department of Energy Science, Sungkyunkwan University, Suwon 440-746, South Korea. E-mail: spark72@skku.edu

ᶜDepartment of Chemistry and Biochemistry, Baylor University, Waco, Texas 76798, United States. E-mail: kevin_shuford@baylor.edu

1 N. Kristian, Y. L. Yu, P. Gunawan, R. Xu, W. Q. Deng, X. W. Liu and X. Wang, *Electrochim. Acta*, 2009, **54**, 4916-4924.

2 W. W. He, X. C. Wu, J. B. Liu, K. Zhang, W. G. Chu, L. L. Feng, X. A. Hu, W. Y. Zbou and S. S. Me, *J. Phys. Chem. C*, 2009, **113**, 10505-10510.

3 C. L. Lee and C. M. Tseng, *J. Phys. Chem. C*, 2008, **112**, 13342-13345.

4 S. J. Guo, L. Wang, W. Wang, Y. X. Fang and E. K. Wang, *J. Colloid Interface Sci.*, 2007, **315**, 363-368.

5 S. Y. Wang, N. Kristian, S. P. Jiang and X. Wang, *Nanotechnology*, 2009, **20**, 025605.

6 Y. Kim, J. W. Hong, Y. W. Lee, M. Kim, D. Kim, W. S. Yun and S. W. Han, *Angew. Chem. Int. Ed.*, 2010, **49**, 10197-10201.

7 R. Narayanan and M. A. El-Sayed, *Nano Lett.*, 2004, **4**, 1343-1348.

8 H. Zhang, M. S. Jin and Y. N. Xia, *Chem. Soc. Rev.*, 2012, **41**, 8035-8049.

9 M. A. Mahmoud and M. A. El-Sayed, *J. Am. Chem. Soc.*, 2010, **132**, 12704-12710.

10 K. S. Lee and M. A. El-Sayed, *J. Phys. Chem. B*, 2006, **110**, 19220-19225.

11 C. X. Yu and J. Irudayaraj, *Anal. Chem.*, 2007, **79**, 572-579.

12 C. L. Nehl and J. H. Hafner, *J. Mater. Chem.*, 2008, **18**, 2415-2419.

13 M. A. Mahmoud and M. A. El-Sayed, *Langmuir*, 2012, **28**, 4051-4059.

14 K. Zhang, Y. J. Xiang, X. C. Wu, L. L. Feng, W. W. He, J. B. Liu, W. Y. Zhou and S. S. Xie, *Langmuir*, 2009, **25**, 1162-1168.

15 J. W. Hong, S. U. Lee, Y. W. Lee and S. W. Han, *J. Am. Chem. Soc.*, 2012, **134**, 4565-4568.

16 H. J. Chen, X. S. Kou, Z. Yang, W. H. Ni and J. F. Wang, *Langmuir*, 2008, **24**, 5233-5237.

17 A. R. Tao, S. Habas and P. D. Yang, *Small*, 2008, **4**, 310-325.

18 M. Min, C. Kim, Y. I. Yang, J. Yi and H. Lee, *Phys. Chem. Chem. Phys.*, 2009, **11**, 9759-9765.

19 B. N. Wanjala, J. Luo, R. Loukrakpam, B. Fang, D. Mott, P. N. Njoki, M. Engelhard, H. R. Naslund, J. K. Wu, L. C. Wang, O. Malis and C. J. Zhong, *Chem. Mater.*, 2010, **22**, 4282-4294.

20 M. L. Personick, M. R. Langille, J. Zhang and C. A. Mirkin, *Nano Lett.*, 2011, **11**, 3394-3398.

21 Y. N. Xia, Y. J. Xiong, B. Lim and S. E. Skrabalak, *Angew. Chem. Int. Ed.*, 2009, **48**, 60-103.

22 L. He, M. D. Musick, S. R. Nicewarner, F. G. Salinas, S. J. Benkovic, M. J. Natan and C. D. Keating, *J. Am. Chem. Soc.*, 2000, **122**, 9071-9077.

23 J. E. Millstone, S. J. Hurst, G. S. Metraux, J. I. Cutler and C. A. Mirkin, *Small*, 2009, **5**, 646-664.

24 X. M. Lu, M. Rycenga, S. E. Skrabalak, B. Wiley and Y. N. Xia, *Annu. Rev. Phys. Chem.*, 2009, **60**, 167-192.

25 J. E. Millstone, W. Wei, M. R. Jones, H. J. Yoo and C. A. Mirkin, *Nano Lett.*, 2008, **8**, 2526-2529.

26 P. Zijlstra, C. Bullen, J. W. M. Chon and M. Gu, *J. Phys. Chem. B*, 2006, **110**, 19315-19318.

27 S. Kim, S. K. Kim and S. Park, *J Am Chem Soc*, 2009, **131**, 8380-8381.

28 M. R. Jones, K. D. Osberg, R. J. Macfarlane, M. R. Langille and C. A. Mirkin, *Chem. Rev.*, 2011, **111**, 3736-3827.

29 Y. G. Sun and Y. N. Xia, *Anal. Chem.*, 2002, **74**, 5297-5305.

30 L. L. Feng, X. C. Wu, L. R. Ren, Y. J. Xiang, W. W. He, K. Zhang, W. Y. Zhou and S. S. Xie, *Chem.-Eur. J.*, 2008, **14**, 9764-9771.

31 S. Jung, L. Liu, K. L. Shuford and S. Park, *J. Phys. Chem. C*, 2013, **117**, 3141-3145.

32 S. Kim, K. L. Shuford, H. M. Bok, S. K. Kim and S. Park, *Nano Lett.*, 2008, **8**, 800-804.

33 M. Grzelczak, J. Perez-Juste, B. Rodriguez-Gonzalez and L. M. Liz-Marzan, *J. Mater. Chem.*, 2006, **16**, 3946-3951.

34 M. Grzelczak, J. Perez-Juste, F. J. G. de Abajo and L. M. Liz-Marzan, *J. Phys. Chem. C*, 2007, **111**, 6183-6188.

35 H. J. Jang, S. Hong and S. Park, *J. Mater. Chem.*, 2012, **22**, 19792-19797.

36 F. R. Fan, D. Y. Liu, Y. F. Wu, S. Duan, Z. X. Xie, Z. Y. Jiang and Z. Q. Tian, *J. Am. Chem. Soc.*, 2008, **130**, 6949-6951.

37 Z. B. Jiao, H. B. Xia and X. T. Tao, *J. Phys. Chem. C*, 2011, **115**, 7887-7895.

38 Y. J. Xiang, X. C. Wu, D. F. Liu, L. L. Feng, K. Zhang, W. G. Chu, W. Y. Zhou and S. S. Xie, *J. Phys. Chem. C*, 2008, **112**, 3203-3208.

39 B. T. Draine, *Astrophys. J.*, 1988, **333**, 848.

40 B. T. Draine and P. J. Flatau, *J. Opt. Soc. Am. A*, 1994, **11**, 1491.

41 J. E. Millstone, S. Park, K. L. Shuford, L. D. Qin, G. C. Schatz and C. A. Mirkin, *J. Am. Chem. Soc.*, 2005, **127**, 5312-5313.

42 B. P. Khanal and E. R. Zubarev, *J. Am. Chem. Soc.*, 2008, **130**, 12634-12635.

43 S. Hong, K. L. Shuford and S. Park, *Chem. Mater.*, 2011, **23**, 2011-2013.

Nanoscale

ARTICLE

Table of Contents
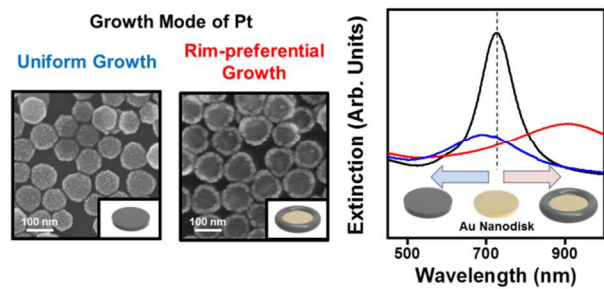
We synthesized shape-controllable Au@Pt nanoplates via rim-preferential or uniform growth of Pt. Depending on the shape of Pt shell, their aspect ratio and surface plasmon resonance band were tunable.